photonics

MDPI

Communication

Localized Effects in Graphene Oxide Systems: A Pathway to Hyperbolic Metamaterials

Grazia Giuseppina Politano

Department of Environmental Engineering, University of Calabria, 87036 Rende, CS, Italy; grazia.politano@unical.it

Abstract: Graphene oxide (GO) has emerged as a carbon-based nanomaterial providing a different pathway to graphene. One of its most notable features is the ability to partially reduce it, resulting in graphene-like sheets through the elimination of oxygen-including functional groups. In this paper, the effect of localized interactions in an Ag/GO/Au multilayer system was studied to explore its potential for photonic applications. GO was dip-coated onto magnetron-sputtered silver, followed by the deposition of a thin gold film to form an Ag/GO/Au structure. Micro-Raman Spectroscopy, SEM and Variable Angle Ellipsometry (VASE) measurements were performed on the Ag/GO/Au structure. An interesting behavior of the GO deposited on magnetron-sputtered silver with the formation of Ag nanostructures on top of the GO layer is reported. In addition to typical GO bands, Micro-Raman analysis reveals peaks such as the 1478 cm^{-1} band, indicating a transition from sp^3 to sp^2 hybridization, confirming the partial reduction of GO. Additionally, calculations based on effective medium theory (EMT) highlight the potential of Ag/GO structures in hyperbolic metamaterials for photonics. The medium exhibits dielectric behavior up to 323 nm, transitions to type I HMM between 323 and 400 nm and undergoes an Epsilon Near Zero and Pole (ENZP) transition at 400 nm, followed by type II HMM behavior.

Keywords: graphene oxide; optical properties; micro Raman

Received: 6 January 2025
Revised: 21 January 2025
Accepted: 28 January 2025
Published: 29 January 2025

Citation: Politano, G.G. Localized Effects in Graphene Oxide Systems: A Pathway to Hyperbolic Metamaterials. *Photonics* **2025**, *12*, 121. https://doi.org/10.3390/photonics12020121

1. Introduction

Photonic metamaterials [1], which enable exact manipulation of light at subwavelength scales, have greatly revolutionized optical technologies over the last years. These materials' special qualities—like improved light–matter interactions, negative refraction and superlensing—have created new opportunities for energy harvesting, imaging and sensing [2]. Recent advancements in metasurface-based photonic devices have further expanded these possibilities by demonstrating improved optical field control, higher efficiency and enhanced damage thresholds, making them particularly suitable for high-power laser applications [3]. Moreover, recent research on terahertz metamaterial absorbers based on Dirac semimetals has shown exceptional tunability and sensitivity [4].

These advances have been made possible in large part by the creation of novel materials and enhanced nanofabrication methods [5]. In addition to optimal designs, the creation of new materials with adjustable optical characteristics and scalable manufacturing techniques are also necessary to achieve such breakthroughs. Because of their remarkable electrical and optical properties, graphene and its derivatives, including graphene oxide (GO) [6], have turned out to be attractive options for incorporation into photonic metamaterials.

Graphene and GO differ in terms of structure and properties. Graphene consists of carbon atoms arranged in a two-dimensional honeycomb lattice with sp^2 hybridization,

which provides it with exceptional electrical conductivity, mechanical strength and thermal properties [7]. Graphene can be synthesized using four main methods. The first method involves chemical vapor deposition (CVD) [8]. The second method is micromechanical exfoliation, commonly known as the 'Scotch tape' [9] or peel-off technique, which originated from earlier work on exfoliating patterned graphite. The third approach utilizes epitaxial growth on insulating substrates like silicon carbide (SiC) [9], while the fourth involves the production of colloidal suspensions [10]. Although graphene has earned a lot of interest due to its many uses, the difficulties associated with mass manufacture prevent it from being used in technology on a significant scale [11]. As an alternative to graphene, GO offers a more approachable and adaptable platform for real-world uses. GO contains both sp^2 and sp^3 hybridized carbon atoms due to the presence of oxygen-containing functional groups such as epoxy, hydroxyl and carboxyl. These functional groups enhance its dispersibility in water but significantly reduce its electrical conductivity compared to pristine graphene [12]. GO can be converted into reduced graphene oxide (RGO) by eliminating oxygen-including functional groups, resulting in graphene-like sheets with restored properties, regaining its electrical conductivity and optical characteristics despite its insulating nature brought on by the breakage of its conjugated electronic structure [13]. However, conventional chemical reduction techniques frequently include dangerous chemicals like hydrazine, which emphasizes the need for alternative scalable and sustainable strategies [14]. In the development of new materials for photonic applications, where environmentally friendly and adjustable procedures are becoming more and more crucial, these alternative reduction techniques may be crucial [15]. Concerning the catalytic reduction of GO, Wu et al. [16] demonstrated that Ag nanoparticles can facilitate the visible-light-driven photocatalytic reduction of GO through the mechanism of Surface Plasmon Resonance (SPR). Furthermore, other important advancements have been reported in this research field. For example, Zhuo et al. [17] described a method for the large-scale production of graphene through the room-temperature reduction of GO, utilizing metal nanoparticles as catalysts. In addition, the γ-ray-assisted synthesis of silver nanoparticle-decorated RGO/Ag represents a promising green approach for the development of advanced materials in energy storage applications, particularly symmetric supercapacitors [18]. The fabrication process has a particular influence on the design of metamaterials for practical applications [19,20]. Magnetron sputtering [21] is a scalable and repeatable method that ensures the consistency required for advanced photonic metamaterials by producing thin films with nanoscale accuracy.

This work focuses on the magnetron sputtering deposition of a multilayer Ag/GO/Au system. Micro-Raman spectroscopy reveals that localized plasmonic interactions between gold and silver enhance electromagnetic field localization at the interface, potentially modifying the optical behavior of GO. This approach highlights a possible alternative to traditional chemical methods for reducing GO, meeting the criteria of being inexpensive and environmentally friendly.

When the Ag/GO interface in the system is examined more closely, some features become apparent. The appearance of silver nanostructures on the GO layer is demonstrated by SEM measurements, generating "hot spots" that are essential for Surface-Enhanced Raman Scattering (SERS). Additionally, effective medium theory (EMT) [22] calculations demonstrate that the GO/Ag combination is a promising candidate for integration into hyperbolic metamaterials. Such metamaterials enable unique optical properties, including negative refraction and enhanced light–matter interactions, opening the door for innovative applications in photonic technologies.

2. Materials and Methods

Deposition of silver thin films (10 nm) was carried out on glass substrates using a DC magnetron sputtering system (Edwards Auto306, West Sussex, UK) under an argon partial pressure of 4.5×10^{-2}, with a base vacuum of 10^{-5} mbar and a cathode power of 10 W for 75 s. The glass substrates were pre-cleaned with a "piranha solution" (hydrogen peroxide and sulfuric acid).

GO films (8 nm) were deposited on the silver thin films using a dip-coating process at 0.33 mm/s. A 2 g/L GO dispersion in water, sourced from "Punto Quantico", was used. Gold thin films (15 nm) were then deposited onto the GO/Ag/glass substrates using the same sputtering system at 4.2×10^{-2} mbar, with a base vacuum of 10^{-5} mbar and a cathode power of 30 W for 55 s. A schematic of the Ag/GO/Au structure is shown in Figure 1.

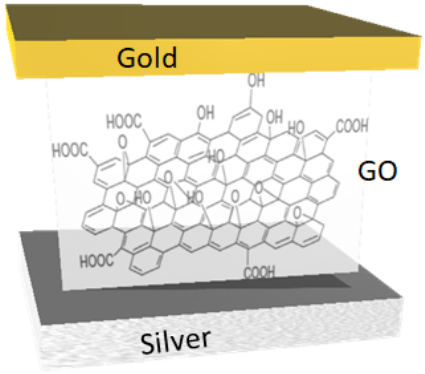

Figure 1. Schematic illustration of the samples.

Micro-Raman spectroscopy was carried out using a Horiba-Jobin Yvon LabRam HR system (Horiba-Jobin Yvon Srl, Piscataway, NJ, USA) with a 532 nm laser and a 100× Mplan Olympus objective. An OD2 filter (1% transmission) was used to minimize thermal effects. SEM analysis was performed with a FEI Quanta FEG 400 ESEM microscope (Eindhoven, The Netherlands).

Optical properties were estimated via Variable Angle Spectroscopic Ellipsometry (VASE) using a Woollam M2000 F (Woollam Co., Lincoln, NE, USA) rotating compensator ellipsometer, covering the photon energy range of [1.3–4.1] eV.

3. Results and Discussion

3.1. Micro-Raman Measurements

The visual investigation of the samples (Figure 2A) reveals that two types of GO deposition are possible. The "light" zones can be associated with a monolayer or few-layer growth. In contrast, the remaining areas appear in varying shades of dark colors.

The formation of some "hot spots" is observed, usually in the "dark" regions of this sample. Hot spots are highly concentrated areas of strong local field enhancement attributed to localized surface plasmon resonance (LSPR) [23]. These regions, found in the gaps of metallic nanostructures, are known to significantly amplify SERS signals [24]. An example of this phenomenon can be observed in Figure 2B. The D and G bands of GO are visible at about 1365 cm^{-1} and 1595 cm^{-1}, correspondingly. Moreover, it is possible to see the second order D + G band (≈2912 cm^{-1}). In addition, several sharp peaks appear at about 1077 cm^{-1}, 1122 cm^{-1}, 1240 cm^{-1}, 1286 cm^{-1}, 1478 cm^{-1} and 1976 cm^{-1}. All these distinct peaks are associated with localized vibrations of molecular groups bound to the GO network and in proximity to metal particles or nanostructures. These "hot spots" arise from the intense plasmonic coupling between the metal and the molecule, leading to an

important enhancement of the Raman signal through the SERS effect. In particular, the peak at about 1478 cm^{-1} can be due to a CH2 deformation vibration; indeed, Aunkor et al. [25] reported that the spectra of RGO display peaks that can be attributed to the CH2 stretching vibration. This observation might confirm that the atomic frame of sp^2 carbon has arisen in RGO, thus indicating the transition from sp^3 (oxidized regions) to sp^2 (graphitic regions) hybridization [25].

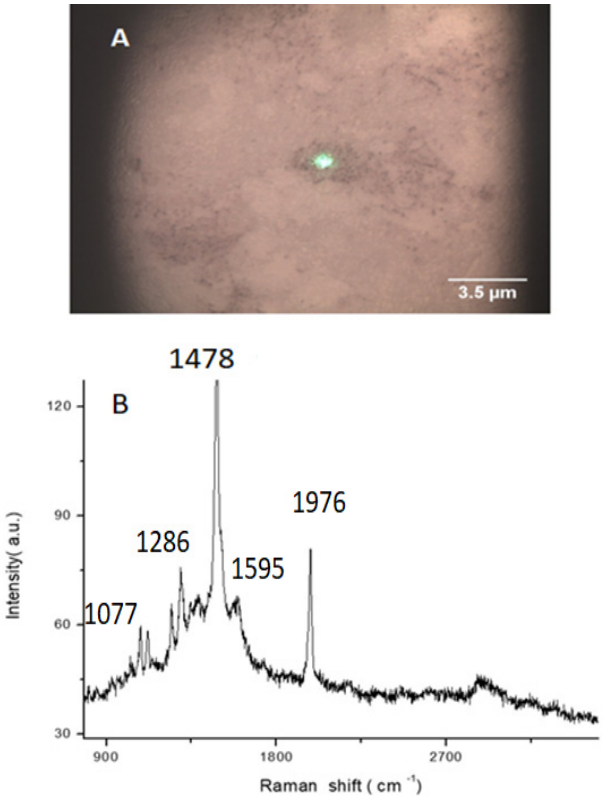

Figure 2. Optical image of a typical region of Ag/Graphene oxide/Au structure. Green laser spot on a dark region (**A**). Raman spectrum on a hot spot of the samples at low laser intensity (OD2 filter) (**B**).

It was observed that the sharp peaks associated with *hot spots* disappeared under high laser power, suggesting thermal effects. To minimize this influence, low-power laser settings were used during the measurements (OD2 filter). While plasmonic effects play a role in enhancing the Raman signal, the potential for laser-induced thermal degradation must also be considered when interpreting these results.

3.2. Morphological SEM Analysis

In Figure 3, sections of the Glass/Ag/GO/Au layer structure were obtained using a secondary electron sensor. In the images, it is possible to see some 40/50 nm Ag nanoparticles covered by a thin film of different chemical compositions that flexibly conform to the nanostructured substrate.

In Figure 4, the glass/Ag/GO sample was studied without the gold coating to explore the Ag/GO interface of the more complex glass/Ag/GO/Au structure.

Figure 4A shows a topography image of the glass/Ag/GO structure acquired by the secondary electron sensor. Some objects (supposedly Ag nanoparticles of 40/50 nm diameters) are visible on the GO surface. Figure 4C shows a magnification of Figure 4A. The same objects were observed with the Back Scattering sensor that highlights an atomic number difference between superficial (brighter) objects, presumably Ag nanoparticles, on a less luminous surface of GO (Figure 4B). Figure 4D shows a magnification of Figure 4B.

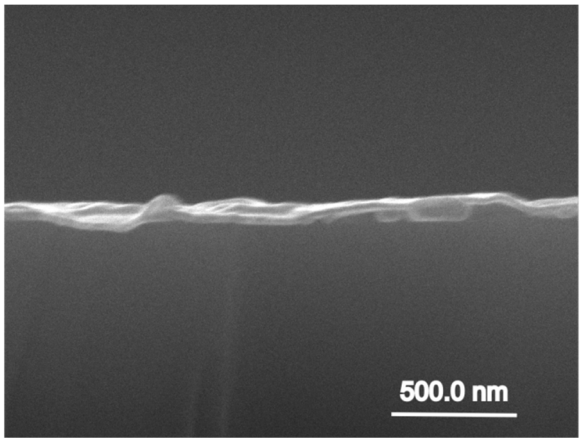

Figure 3. Higher magnification ESEM image of glass/Ag/GO/Au layer samples. It is possible to see some Ag nanoparticles below the graphene oxide and the Au thin films obtained using a secondary electron detector.

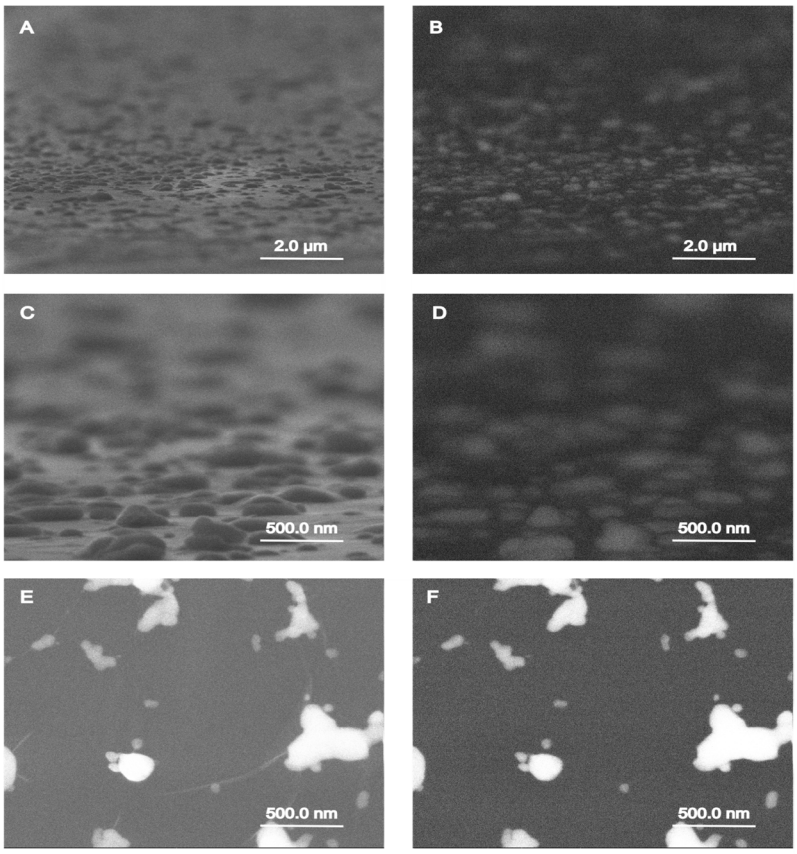

Figure 4. ESEM images of the surface topography of a glass/Ag/graphene oxide sample. Images (**A**,**C**,**E**) were obtained using a secondary electron detector; images (**B**,**D**,**F**) were acquired by a backscattered electron detector. Some objects, supposedly Ag nanoparticles of 40/50 nm diameters, are visible on the graphene oxide surface (**A**) and related magnification (**C**). The backscattered electron detector highlights the atomic number difference between superficial (brighter) objects, presumably Ag nanoparticles, and a less luminous graphene oxide background film. The Ag nanoparticles pierce the graphene oxide layer in some places (**E**,**F**); in (**E**), we can also see the cleavage lines, which start where the Ag nanoparticles break the graphene oxide layer.

An example of cleavage across the Ag/GO interface is visible in Figure 4E (see, in particular, the scratches due to the silver nanoparticles below the GO film). Figure 4F reports the corresponding backscattering image.

The glass/Ag/GO system is very complex, and there are zones of samples in which the GO layer adjusts elastically to the Ag nanoparticles.

Figure 5A, for instance, shows the topography acquired by the secondary electron sensor on a surface of GO dip-coated on 10 nm magnetron-sputtered Ag. Objects of about 40/50 nm diameter are visible on the surface, but they are thought to be a deformation of the GO film induced by Ag nanoparticles grown in the underlying surface, which did not perforate the GO layer, as confirmed by the corresponding image. Figure 5B was acquired by the backscattering sensor. The behavior of the complex interface Ag/GO, never reported before, requires further studies because a greater understanding could open the way for several applications. The dispersion of Ag nanoparticles within the thin Ag film, along with their potential detachment from the surface, leads to varying interactions with molecular groups. In this study, this phenomenon may explain the formation of the "hot spots" detected using micro-Raman spectroscopy.

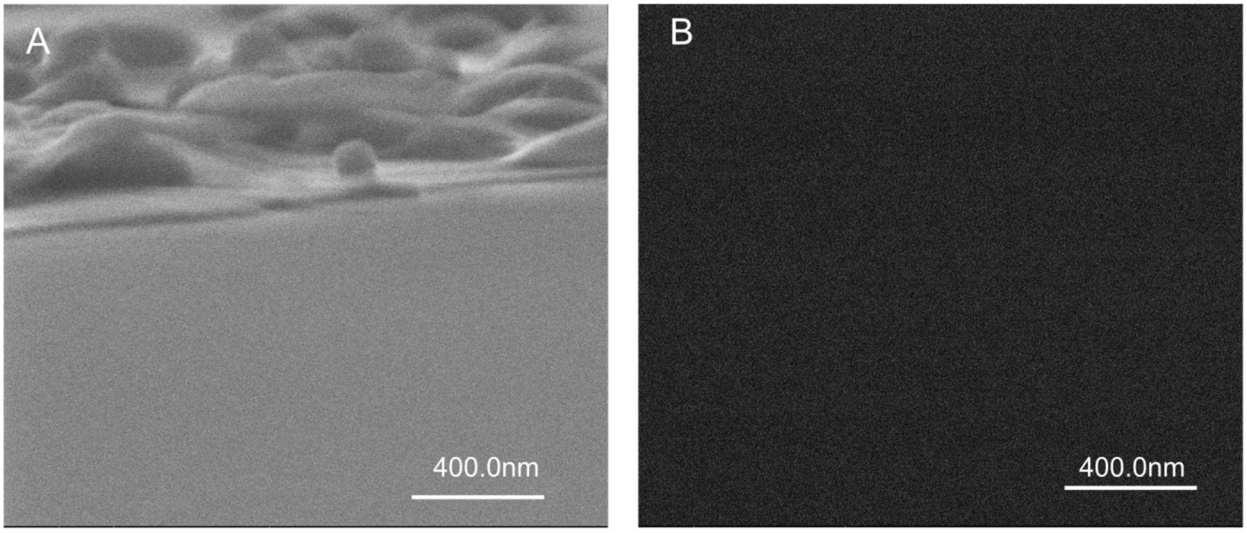

Figure 5. ESEM images of a glass/Ag/graphene oxide sample acquired by a secondary (**A**) and a backscattered (**B**) electron detector. The images show the same morphology as those reported in Figure 4, but the backscattering image reveals that the chemical composition of the surface is homogeneous. In this case, the Ag nanoparticles can curve the graphene oxide film, but they do not pierce the graphene oxide layer.

3.3. Variable Angle Spectroscopic Ellipsometry Measurements

VASE was used to check the average thickness of the thin films. The analysis of the ellipsometric data requires a multilayer optical model of the samples.

The ψ and Δ spectra were measured at different angles of incidence (50°–70°) to increase the accuracy of layer modeling.

The model was obtained using the superposition of a layer of glass (1 mm), Ag (10 nm) and EMA (Effective Medium Approximation) model between the optical constants of GO and that of silver (8 nm) and Au (15 nm).

In Figure 6A,B, the generated and experimental data of the ψ and Δ spectra are reported for different angles of incidents in the [1.3–4.1] eV photon energy range for the glass/Ag/GO/Au structure.

It is worth noting that the spot size of the light beam used in spectroscopic ellipsometry is typically several millimeters, which means a bigger spot size in comparison with Raman spectra and SEM analysis. However, important information can be deduced from Figure 6A,B.

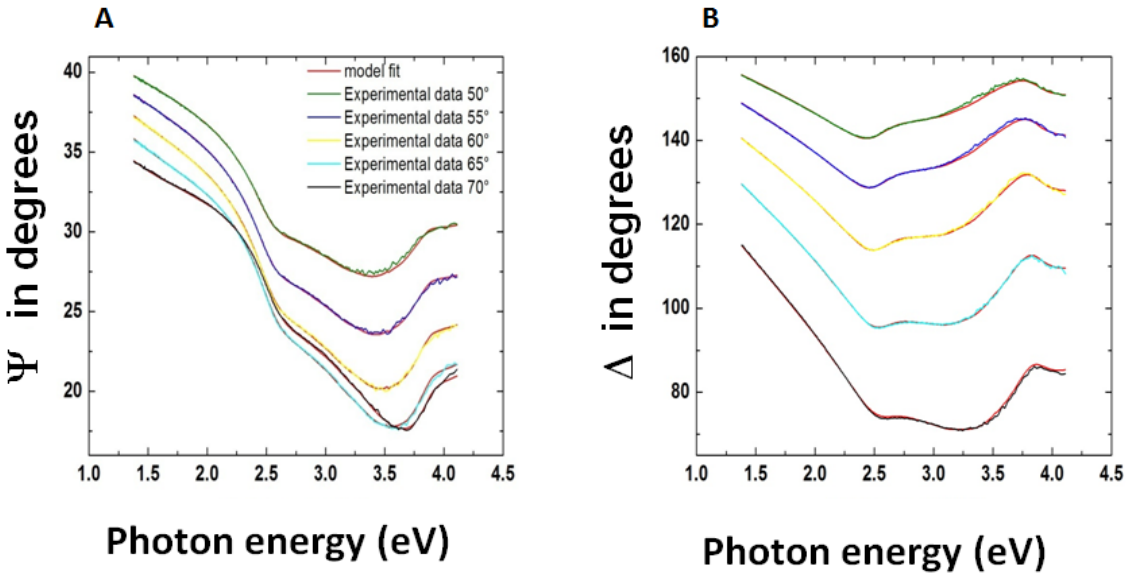

Figure 6. Experimental and model-generated ellipsometric ψ (**A**) and Δ (**B**) data fits at five angles of incidences for the glass/Ag/GO/Au structure.

In Figure 7A, the estimated dispersion laws of the GO sample deposited with the dip-coating technique on magnetron-sputtered Ag/glass substrate by ellipsometry characterization are reported in the [1.3–4.1] eV photon energy range.

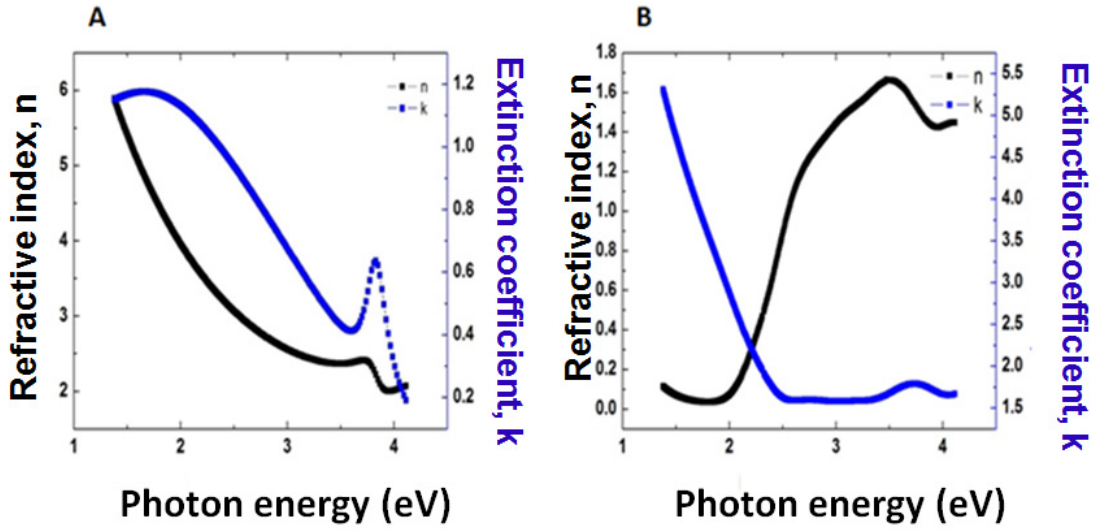

Figure 7. Estimated dispersion laws of the glass/Ag/GO structure (**A**) and of the glass/Ag/GO/Au structure (**B**). The curves show the index of refraction (black lines) and the extinction coefficient (blue lines).

The model was obtained using the superposition of a layer of glass (1 mm), Ag (10 nm) and an EMA model, which mixes the Cauchy optical constants of GO and those of silver (8 nm). The EMA model was selected due to the nanostructured nature of the interface, and its validity has been supported by the consistency between modeled and experimental ellipsometric data. The model indicates the formation of a layer of GO with mixed silver features; for example, we find an oscillator at 3.8 eV, which can be attributable to the volume plasmon of Ag [26]. The mixed properties between silver and GO are consistent with the observed behavior in SEM images. In Figure 7B, the dispersion laws are reported in the [1.3–4.1] eV photon energy range. The optical constants are very similar to those of

gold [27]; hence, the thin gold film adjusts elastically on the glass/Ag/GO sample (as can be seen in Figure 3) without modifying its overall optical behavior.

3.4. Potential Application in Hyperbolic Metamaterials

A potential application has been identified for films composed of GO dip-coated on magnetron-sputtered silver as hyperbolic metamaterials.

A hyperbolic metamaterial [28] is an anisotropic medium characterized by uniaxial dielectric tensor components:

$\varepsilon_{xx} = \varepsilon_{yy} = \varepsilon_{\parallel}$ and $\varepsilon_{yy} = \varepsilon_{\perp}$, which can be approximated using effective medium theory (EMT):

$$\varepsilon_{\parallel} = \frac{t_m \varepsilon_m + t_d \varepsilon_d}{t_m + t_d} \quad (1)$$

$$\varepsilon_{\perp} = \frac{\varepsilon_m \varepsilon_d (t_m + t_d)}{t_m \varepsilon_d + t_d \varepsilon_m} \quad (2)$$

In Equations (1) and (2), (t_d, ε_d) and (t_m, ε_m) are the thickness and dielectric permittivity of dielectric and metal, respectively.

Figure 8 presents an EMT simulation based on the optical constants of 20 nm thick graphene oxide (GO) and 20 nm thick magnetron-sputtered silver. The results demonstrate the theoretical feasibility of achieving the rare coexistence of two opposite anisotropies, type I and type II, within the same metamaterial. This coexistence is characterized by a zero dielectric or metal gap separating the two anisotropic states.

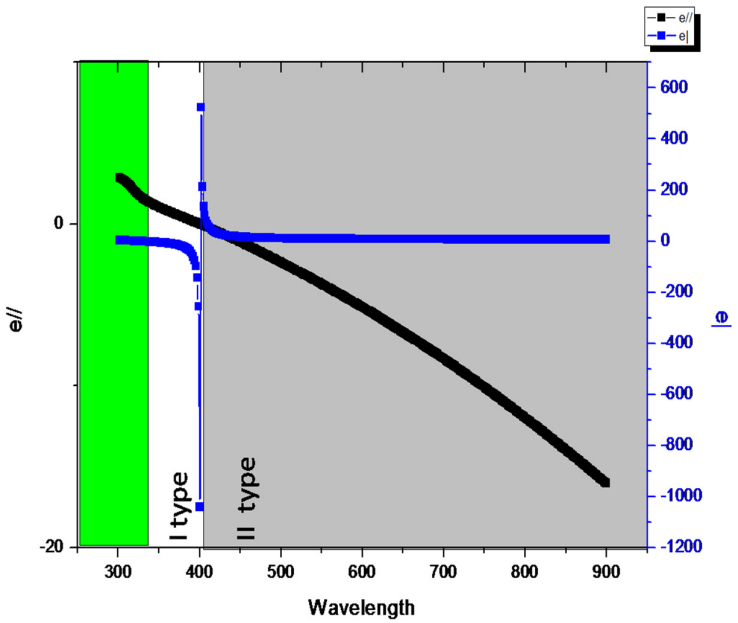

Figure 8. The effective medium theory (EMT) applied to alternating GO/Ag multilayers. The black curve represents the real part of the parallel component of epsilon, while the blue curve corresponds to the perpendicular component of the entire structure.

For type I hyperbolic metamaterials HMM ($\varepsilon_{\parallel} > 0$ and $\varepsilon_{\perp} < 0$), the structure exhibits dielectric properties in the xy plane and metallic properties along the $\varepsilon_{\perp}$ direction, while the isofrequency surfaces assume the shape of an open-bounded hyperboloid. In this configuration, the isofrequency surfaces take the form of an open, bounded hyperboloid. Conversely, in type II HMM, the behavior is reversed and the isofrequency surface transitions to a continuous hyperboloid.

As illustrated in Figure 8, the medium exhibits dielectric behavior up to a wavelength of 323 nm (green area), as both $\varepsilon_{\parallel}$ and $\varepsilon_{\perp}$ are positive. Between 323 nm and 400 nm (white

area), $\varepsilon_{\parallel} > 0$ while $\varepsilon_{\perp} < 0$, resulting in the emergence of a type I HMM region. At $\lambda = 400$ nm, the ε_{NZP} (Epsilon Near Zero and Pole) behavior obviously manifests a strong discontinuity in $\varepsilon_{\perp}$, passing from a very high negative value (virtually $-\infty$) to a very high positive one (virtually $+\infty$) while simultaneously, $\varepsilon_{\parallel} = 0$. The HMM transitions to type II behavior at $\lambda > 400$ nm (grey area).

The results presented here emphasize the critical role of the reduction process in tuning the optical properties of the Ag/GO/Au structure. Raman spectroscopy confirms the transition from sp^3 to sp^2 hybridization, indicating partial reduction of GO, which is essential for enhancing conductivity and optimizing its performance in photonic applications. However, despite the environmental advantages of the plasmonic reduction approach compared to conventional chemical methods, achieving uniformity and reproducibility on a larger scale is still a limiting factor. In addition, the theoretical model confirms the potential of the application of Ag/GO structures in hyperbolic metamaterials; nevertheless, practical implementation of these metamaterials faces challenges related to fabrication precision and consistency, which must be addressed to fully exploit their potential in applications such as imaging, sensing and waveguiding at the nanoscale.

4. Conclusions

This study explores the potential of Ag/GO/Au structures for photonic applications, particularly their suitability as hyperbolic metamaterials. Gold is used to ensure chemical stability and enhance plasmonic coupling with silver. Micro-Raman analysis detects additional peaks beyond the typical GO bands, including a peak at 1478 cm^{-1} attributed to CH_2 deformation vibrations, indicating the transition from sp^3 (oxidized) to sp^2 (graphitic) carbon hybridization. SEM images reveal that the Au film conforms elastically to Ag nanostructures (~40–50 nm), potentially contributing to the observed "hot spots" in Raman measurements. The dispersion properties of the structure align with the SEM observations, with the Au layer maintaining the overall optical behavior, while the GO/Ag interface presents complexity. Ellipsometry suggests a GO layer incorporating silver features, with an oscillator at 3.8 eV linked to Ag volume plasmons. Theoretical analysis indicates that by optimizing Ag and GO thicknesses, these structures can act as multilayer hyperbolic metamaterials, exhibiting simultaneous type I and type II anisotropies, separated by a zero dielectric or metal gap. While still theoretical, these findings present significant experimental challenges and promising applications in plasmonics and metamaterials.

Funding: This research received no external funding.

Institutional Review Board Statement: Not applicable.

Informed Consent Statement: Not applicable.

Data Availability Statement: The data are contained within the article.

Conflicts of Interest: The author declares no conflict of interest.

Abbreviations

The following abbreviations are used in this manuscript:

GO	Graphene oxide
EMT	Effective medium theory
RGO	Reduced graphene oxide
VASE	Variable Angle Spectroscopic ellipsometry
EMA	Effective Medium Approximation
ENZP	Epsilon Near Zero and Pole

References

1. Wang, Z.; Cheng, F.; Winsor, T.; Liu, Y. Optical chiral metamaterials: A review of the fundamentals, fabrication methods and applications. *Nanotechnology* **2016**, *27*, 412001. [CrossRef] [PubMed]
2. Ma, W.; Cheng, F.; Xu, Y.; Wen, Q.; Liu, Y. Probabilistic Representation and Inverse Design of Metamaterials Based on a Deep Generative Model with Semi-Supervised Learning Strategy. *Adv. Mater.* **2019**, *31*, 1901111. [CrossRef] [PubMed]
3. Wang, Q.; Fang, Y.; Meng, Y.; Hao, H.; Li, X.; Pu, M.; Ma, X.; Luo, X. Vortex-field enhancement through high-threshold geometric metasurface. *Opto-Electron. Adv.* **2024**, *7*, 240112. [CrossRef]
4. Zeng, Z.; Liu, H.; Zhang, H.; Cheng, S.; Yi, Y.; Yi, Z.; Wang, J.; Zhang, J. Tunable ultra-sensitive four-band terahertz sensors based on Dirac semimetals. *Photonics Nanostruct. Fundam. Appl.* **2025**, *63*, 101347. [CrossRef]
5. Chi, T.; Somers, P.; Wilcox, D.A.; Schuman, A.J.; Iyer, V.; Le, R.; Gengler, J.; Ferdinandus, M.; Liebig, C.; Pan, L.; et al. Tailored thioxanthone-based photoinitiators for two-photon-controllable polymerization and nanolithographic printing. *J. Polym. Sci. Part B Polym. Phys.* **2019**, *57*, 1462–1475. [CrossRef]
6. Politano, G.G. Optimizing Graphene Oxide Film Quality: The Role of Solvent and Deposition Technique. *C* **2024**, *10*, 90. [CrossRef]
7. Urade, A.R.; Lahiri, I.; Suresh, K.S. Graphene Properties, Synthesis and Applications: A Review. *JOM* **2023**, *75*, 614–630. [CrossRef] [PubMed]
8. Saeed, M.; Alshammari, Y.; Majeed, S.A.; Al-Nasrallah, E. Chemical Vapour Deposition of Graphene—Synthesis, Characterisation, and Applications: A Review. *Molecules* **2020**, *25*, 3856. [CrossRef]
9. Han, Y.-C.; Yin, S.-H.; Zheng, J.-R.; Hu, Y.-F.; Sun, L.; Zhang, L.; Tian, Z.-Q.; Yi, J. Epitaxial Growth of Graphene on SiC by Thermal Shock Annealing Within Seconds. *Adv. Funct. Mater.* **2024**, *34*, 2307298. [CrossRef]
10. Lee, S.J.; Huh, H.K.; Kwon, D.H. Energy dissipation of graphene colloidal suspension droplets impacting on solid substrates. *RSC Adv.* **2014**, *4*, 7216–7224. [CrossRef]
11. Politano, G.G. Optical Properties of Graphene Nanoplatelets on Amorphous Germanium Substrates. *Molecules* **2024**, *29*, 4089. [CrossRef] [PubMed]
12. Mohammed, S. Graphene oxide: A mini-review on the versatility and challenges as a membrane material for solvent-based separation. *Chem. Eng. J. Adv.* **2022**, *12*, 100392. [CrossRef]
13. Kurian, M. Recent progress in the chemical reduction of graphene oxide by green reductants–A Mini review. *Carbon Trends* **2021**, *5*, 100120. [CrossRef]
14. Cao, K.; Tian, Z.; Zhang, X.; Wang, Y.; Zhu, Q. Green preparation of graphene oxide nanosheets as adsorbent. *Sci. Rep.* **2023**, *13*, 9314. [CrossRef] [PubMed]
15. Joshi, R.; De Adhikari, A.; Dey, A.; Lahiri, I. Green reduction of graphene oxide as a substitute of acidic reducing agents for supercapacitor applications. *Mater. Sci. Eng. B* **2023**, *287*, 116128. [CrossRef]
16. Wu, T.; Liu, S.; Luo, Y.; Lu, W.; Wang, L.; Sun, X. Surface plasmon resonance-induced visible light photocatalytic reduction of graphene oxide: Using Ag nanoparticles as a plasmonic photocatalyst. *Nanoscale* **2011**, *3*, 2142–2144. [CrossRef] [PubMed]
17. Zhuo, Q.; Gao, J.; Peng, M.; Bai, L.; Deng, J.; Xia, Y.; Ma, Y.; Zhong, J.; Sun, X. Large-scale synthesis of graphene by the reduction of graphene oxide at room temperature using metal nanoparticles as catalyst. *Carbon N. Y.* **2013**, *52*, 559–564. [CrossRef]
18. Kodous, A.S.; Taha, E.O.; El-Maghraby, D.F.; Hassana, A.A.; Atta, M.M. Gamma radiation assisted green synthesis of hesperidin-reduced graphene oxide nanocomposite targeted JNK/SMAD4/MMP2 signaling pathway. *Sci. Rep.* **2024**, *14*, 11535. [CrossRef]
19. Fan, Z.; Li, B.; Zhou, S.; Huang, G. Terahertz Meta-Mirror with Scalable Reflective Passband by Decoupling of Cascaded Metasurfaces. *Photonics* **2024**, *11*, 796. [CrossRef]
20. Zhang, Y.; Feng, R.; Shi, B.; Li, X.; Gao, Y.; Gao, W.; Jia, Q.; Sun, F.; Cao, Y.; Ding, W. Ultra-Compact Reflective Waveguide Mode Converter Based on Slanted-Surface and Subwavelength Metamaterials. *Photonics* **2024**, *11*, 838. [CrossRef]
21. Sasani Ghamsari, M. Development of Thin Film Fabrication Using Magnetron Sputtering. *Metals* **2023**, *13*, 963. [CrossRef]
22. Shekhar, P.; Atkinson, J.; Jacob, Z. Hyperbolic metamaterials: Fundamentals and applications. *Nano Converg.* **2014**, *1*, 14. [CrossRef]
23. Mayer, K.M.; Hafner, J.H. Localized Surface Plasmon Resonance Sensors. *Chem. Rev.* **2011**, *111*, 3828–3857. [CrossRef]
24. Thuy An, N.; Kieu Thi Ta, H.; Van Hoang, D.; Phung, V.-D.; Hoa Thi Tran, N.; Thang Phan, B. Multilayer Graphene Oxide-Silver Nanoparticles for Stable, Highly Sensitive, and Reusable SERS Platforms. *ChemNanoMat* **2023**, *9*, e202200516. [CrossRef]
25. Aunkor, M.T.H.; Mahbubul, I.M.; Saidur, R.; Metselaar, H.S.C. The green reduction of graphene oxide. *RSC Adv.* **2016**, *6*, 27807–27828. [CrossRef]
26. Zacharias, P.; Kliewer, K.L. Dispersion relation for the 3.8 eV volume plasmon of silver. *Solid State Commun.* **1976**, *18*, 23–26. [CrossRef]

27. Johnson, P.B.; Christy, R.W. Optical Constants of the Noble Metals. *Phys. Rev. B* **1972**, *6*, 4370–4379. [CrossRef]
28. Cai, W.; Shalaev, V.M. *Optical Metamaterials*; Springer: Berlin/Heidelberg, Germany, 2010; Volume 10.